REDUCED ORDER OPTIMIZATION OF INTERNAL CHANNEL HEAT SINK DESIGNS

BY

ANIKET AJAY LAD

THESIS

Submitted in partial fulfillment of the requirements
for the degree of Master of Science in Mechanical Engineering
in the Graduate College of the
University of Illinois Urbana-Champaign, 2022

Urbana, Illinois

Adviser:

Associate Professor Nenad Miljkovic

ABSTRACT

The recent growth in electronics power density has created a significant need for effective thermal management solutions. Liquid-cooled heat sinks or cold plates are typically used to achieve high volumetric power density cooling. A natural trade-off exists between the thermal and hydraulic performance of a cold plate, creating an opportunity for design optimization. Current design optimization methods rely on computationally expensive and time-consuming computational fluid dynamics (CFD) simulations. Here, we develop a rapid design optimization tool for liquid cooled heat sinks based on reduced order models for the thermal-hydraulic behavior. Flow layout is expressed as a combination of simple building blocks on a divided coarse grid. The flow layout and geometrical parameters are incorporated to optimize designs that can effectively address heterogeneous cooling requirements within electronics packages. Layout optimization problem of assigning flow blocks on elements of the coarse grid is solved using discrete optimization method. Modifying the expression of flow block in terms of design variables and evaluating non-trivial objective function for partially complete flow layouts coupled with a multi-start approach to improve the probability of finding flow layouts with optimal performance. Gradient-based optimizer enables rapid optimization of internal diameters of the flow blocks for a given flow layout in geometry optimization.

ACKNOWLEDGMENTS

I wish to express sincere gratitude to Professor Nenad Miljkovic, for his guidance and mentoring making this project possible. I would also like to thank Professors William King and Kai James for their support and collaboration with this work. In addition, special thanks to my colleagues in Energy Transport Research Lab for providing valuable inputs and help. I thank Professor James Allison for teaching me the concepts that formed the foundation of this work.

I acknowledge the funding support from the National Science Foundation Engineering Research Center for Power Optimization of Electro-Thermal Systems (POETS) under cooperative agreement EEC-1449548. Special thanks to Jodi Gritten, Owen Doyle, and Dr. Jessica Perez for helping in my academic and professional growth.

Finally, I would like to thank my parents, my sister and all other family members and friends for their love and support. Their confidence in me will always be my greatest source of motivation.

To my parents

TABLE OF CONTENTS

LIST OF FIGURES

NOMENCLATURE

GA	Genetic Algorithm
CFD	Computational Fluid Dynamics
TO	Topology Optimization
d	Channel hydraulic diameter (m)
v	Average flow velocity (m s^{-1})
L	Flow block size/length (m)
f	Friction factor
Re	Reynolds Number
C_p	Specific heat (J kg^{-1} K^{-1})
T	Temperature (℃)
h	Heat transfer coefficient (W m^{-2} K^{-1})
A	Area (m^2)
S	Conduction Shape Factor (m)
Pr	Prandtl Number
Nu	Nusselt Number
k	Thermal Conductivity (W m^{-1} K^{-1})
$q"$	Heat flux (W m^{-2})
P	Pressure (Pa)
$\dot{m}$	Mass flow rate (kg s^{-1})
$\dot{Q}$	Volume flow rate (m^3 s^{-1})
K	Friction coefficient
C	Heat transfer rate (W K^{-1})

Greek Symbols

ΔP	Pressure drop (Pa)
ρ	Density (kg m^{-3})
μ	Dynamic viscosity (N s m^{-2})
ϵ	Roughness (m)

Θ	Thermal resistance (°C W^{-1})

Subscripts

in	Inlet
out	Outlet
f	Fluid
s	Solid
eff	Effective
c	Cross-section
l	Lateral
top	Top surface
s, max	Surface maximum
s, dev	Surface standard deviation
amb	Ambient
etof	Element heated surface to fluid
etonb	Heated surface element to neighbor
etoamb	Heated surface element to ambient

CHAPTER 1: INTRODUCTION

Electrified transportation has seen tremendous increase over the last decade. This growth is supported by miniaturization of the power electronics making their integration with the onboard traction systems possible. The rapid densification of electronic systems as evident from the International Technology Roadmap for Semiconductors (ITRS) [1] has increased the demand for effective heat dissipation. The trend seen in Figure 1 showcases the increase in the power levels of onboard electronics with the degree of transportation electrification [2]. Thermal management is a roadblock to further miniaturization of electronics considering safe operating condition requirements as well as performance degradation at elevated temperatures within active and passive components.

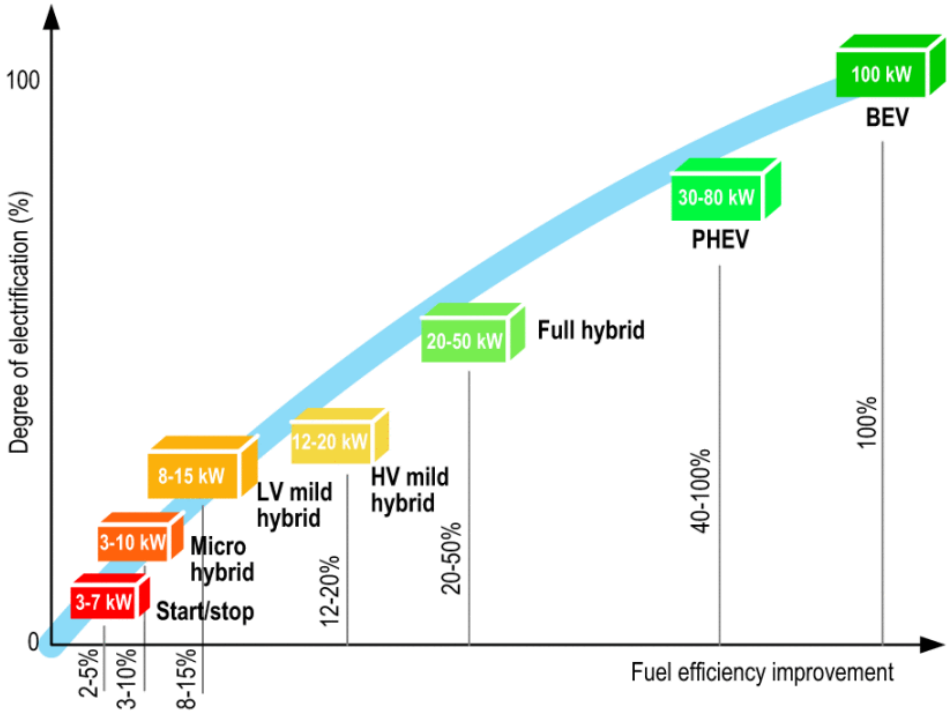

Figure 1.1 Electrified transportation power level trend with degree of electrification [2]

Traditional thermal management solutions employing ambient air as the primary cooling medium are unable to cater to the heat flux rates in highly dense electronics systems. Traditional air-cooled heat sinks are limited in their ability to remove high heat fluxes (>10 W/cm^2 [3]) while maintaining device temperatures within threshold limits to prevent failure [4]. Heat sinks using single phase liquids as coolants show significant improvement in thermal performance due to better coolant thermal properties compared to air. Effective cooling performance and simplicity has popularized the application of single-phase liquid cooled thermal management approaches for electronics cooling [5]. Channelized coolant flow in liquid heat sinks known as cold plates has been employed for numerous electronics cooling applications.

Seminal work on microchannel heat sinks by Tuckerman and Pease [6] demonstrated the potential of liquid cooling solutions for high heat flux removal. Enhancement in the heat transfer performance mapped in terms of the low thermal resistance of 0.1 (^{o}C·cm^2)/W comes at the cost of high pressure drop approaching 2 bar, thus increasing demand for pumping power. Many researchers have investigated liquid cooled heat sink performance for a range of design and operating conditions using experimental [7]–[9], analytical [10]–[13] and numerical approaches [14]–[16]. Results of these studies have guided the design process for liquid cooled systems. Parametric modeling [17]–[19] of performance parameters with respect to design variables including geometric dimensions and flow boundary conditions has provided means for design optimization[20]–[24]. Experimental approaches have yielded the most accurate results for performance modeling but are restrictive in terms of the number of design points that can be considered due to the cost and time required in setting up the experiments for different design variations. Numerical simulations using fluid flow and conjugate heat transfer analysis enable investigation of the necessary performance parameters. Numerical studies however need to be

supported with mesh refinement and experimental validation for ensuring accuracy of the obtained results. Even though parametric studies are a proven tool for design optimization, their scope is limited in terms of design variables available for consideration. This limitation often fails to capture the complete flexibility within the design domain. Implementation of custom channel designs and flow layouts for increasing the heat transfer performance by enhancing flow mixing [25]–[30] is instrumental for designing high performance thermal management systems. Most past studies are constrained in a way that leads to optimization of hyper-specific designs. While providing utility at optimizing those designs, there is a need for additional research that allows for broader search of the design space and consideration of different design architectures.

Inspired by exciting developments in its application to solve problems in structural mechanics, topology optimization (TO) has been adapted for designing high performance heat sinks [31]–[33]. More recently, TO has been adopted for the design of liquid cooled heat sinks [34]–[39]. TO uses numerical simulations and sensitivity calculations for every iteration in the optimization search, which can be computationally expensive and time-consuming. Published research investigated design improvement and optimization of liquid cooled heat sinks most focuses on overall heat transfer performance at a given boundary. In practice, liquid cooled heat sinks can be subject to spatially heterogeneous temperature profiles, resulting in non-uniform heat fluxes and thermal stresses within electronics packages and reduced reliability [40], [41]. Although the challenges associated with device-to-device temperature gradients have been addressed in specific studies focusing on targeted hot-spot cooling [42]–[44], seldom do these studies entail design optimization.

Thermal and hydraulic performance along with the volume and mass of the thermal management solution at the component level as well as the auxiliary component and system level

forms a crucial part of many multi-disciplinary, multi-objective optimization for electro-thermal systems [45]–[48]. Electro-thermal co-design applications use computationally efficient modeling approaches [47], with simplifying assumptions for thermal performance calculations. Temporal and computational resource requirements of existing thermal design optimization approaches using high-fidelity numerical simulations restrict their integration with electro-thermal co-design packages. There is a need for a rapid modeling and optimization for thermo-fluidic parameters of liquid cooled heat exchangers for ensuring true co-design optimization of electric power conversion systems.

This thesis proposes a reduced order design optimization approach for liquid cooled heat sinks/cold plates. To accomplish the task of rapid optimization, a performance estimation approach is used where the fluid flow layout is broken down into flow blocks which form elements divided into a coarser two-dimensional (2D) grid consisting of elementary fluid flow blocks. The governing mass, momentum, and energy equations for fluid flow and heat transfer within fluid and solid domains [49], [50] are solved to obtain the performance of the design in terms of thermal resistance, pressure drop and temperature deviation on the surface heated by electronics components. The optimization process is further broken down into the sub-problems finding the fluid flow layout for given domain information and boundary conditions. Followed by the search for optimal flow layout, geometrical parameters for individual flow blocks considered as design variables for optimization of thermal-hydraulic performance parameters. The sequential layout and geometry optimization on a discretized domain leads to a rapid design optimization of the cold plate.

The rest of this thesis is organized as follows. Chapter 2 describes the domain reduction and optimization approach. Chapter 3 summarizes the modeling approach with special emphasis

on the underlying assumptions. Chapter 4 explains the layout optimization approach using the discrete optimization methods. Chapter 5 describes the geometry optimization. Chapter 6 discusses the need and directions for future work followed by Chapter 7 which concludes the thesis.

CHAPTER 2: DOMAIN REDUCTION AND OPTIMIZATION APPROACH

Cold plate designs with a continuous flow path having fixed inlet and outlet locations is considered in this work. Figure 2.1a represents an exemplary commercial-off-the-shelf (COTS) [51] four-pass cold plate design used for a variety of electronics cooling applications. Electronics components mounted on the surface of such cold plate generate the heat dissipation. The internal channels of the cold plate provide the flow path for the coolant which removes the heat generated by the electronics. The design of the cold plate can be represented in terms of the flow path of the coolant and the diameter of the internal channel at different locations. Effect of these design parameters can be observed on the performance metrics of the cold plate including the thermal parameters like the heated surface temperature and hydraulic parameters like the total pressure drop observed by the coolant in the cold plate.

To simplify the performance evaluation, cold plate design can be broken down into a series of simple flow blocks by dividing the geometry into a coarse grid as shown in Figure 2.1b. Each grid element consists of a unique flow block. The flow blocks for the cold plate design with non-parallel (series) flow can be categorized as straight blocks or elbows which are represented in Figure 2.1c. Dividing the cold plate into discrete blocks allows solving for flow equations in individual blocks simplifying the performance metrics calculation. Additionally, dividing the domain into a grid allows for specifying unique flow blocks, internal diameters, and heat dissipation values for every grid element. This approach provides an effective way of modeling the cold plate having complex internal channels with heterogeneous loss profiles often encountered in electronics cooling applications. Increasing number of discretized elements however results in complex and unrealizable designs along with higher computational costs for modeling and optimization.

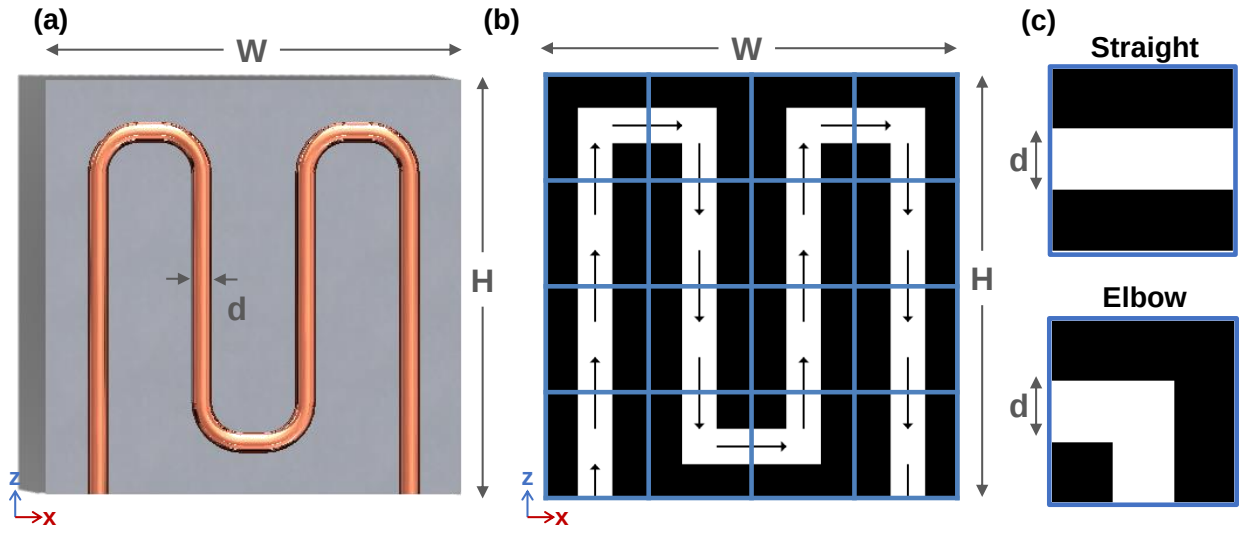

Figure 2.1 (a) Schematic of a commercial standard cold plate design for electronics cooling. (b) Top view of the cold plate domain divided into a coarse grid (blue divider lines) using (c) simplified flow blocks forming elements for cold plate design. Black arrows indicate flow direction, while black coloring represents the solid domain and white coloring represents the fluid domain. Schematics not to scale.

The reduced order modeling approach allows for rapid evaluation of the cold plate performance parameters for any given design. This is leveraged in the design optimization framework to rapidly generate the optimal design for any given set of boundary conditions. Figure 2.2 describes the optimization process. First, the layout optimization is performed based on specified inlet and outlet locations for the coolant flow and the discretized grid size. The layout optimization process involves finding a unique flow block for each grid element, making it an inherently discrete problem. Therefore, discrete optimization methods are employed for layout optimization. Following this, the geometry of the optimal layout, expressed in terms of individual element diameters is optimized to conclude the design optimization process. The continuous nature of the performance parameters with respect to the diameters allows for the use of gradient based optimization solvers for geometry optimization.

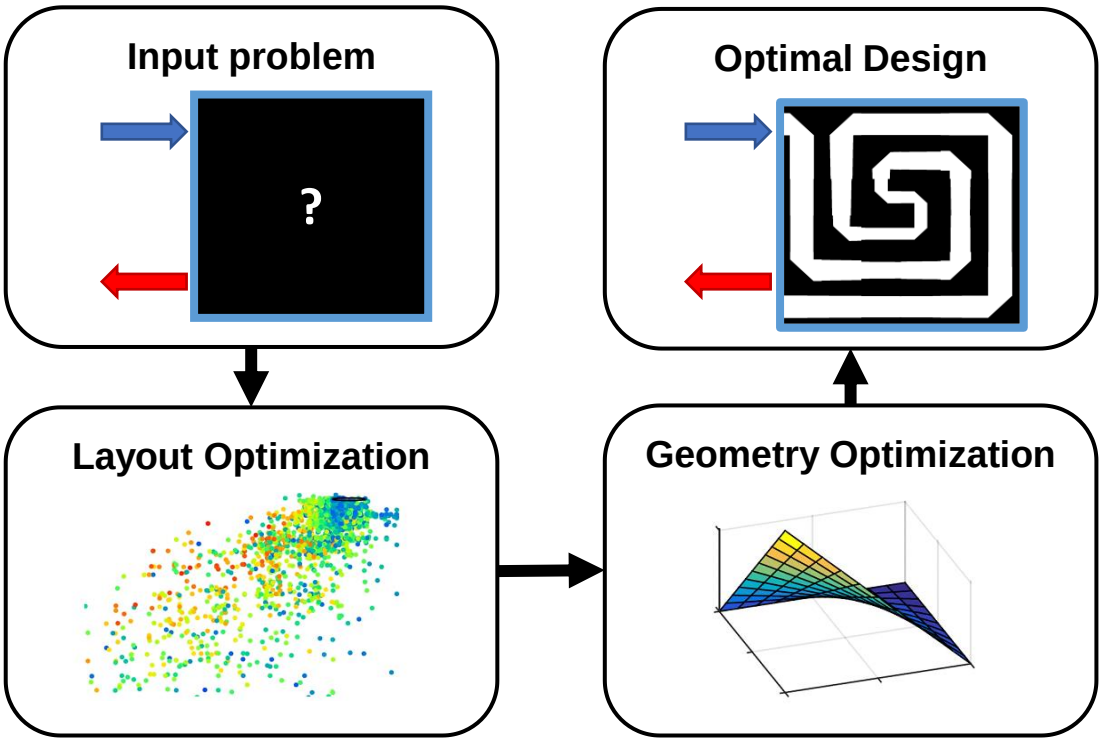

Figure 2.2 Cold plate design optimization approach including layout optimization for a given domain followed by geometry optimization on the optimal layout

Heated surface temperature and the inlet to outlet pressure drop of the cold plate are used as the optimization objectives. The thermal and hydraulic parameters often form competing objectives. For example, a layout with low number of active elements circulates coolant through a limited number of grid elements and thus has a lower pressure drop compared to a design which has more flow blocks covering a longer path in the grid. At the same time, due to the lack of coolant circulation through the complete design, the heated surface temperature is higher. This trade-off leads to non-trivial optimal designs for any given combination of the temperature and pressure drop objectives.

CHAPTER 3: THERMOFLUIDIC PERFORMANCE MODELING

For any given cold plate design expressed in terms of a flow layout and diameters on a coarse grid, the performance modeling is used to obtain the metrics used as optimization objectives and constraints. The thermal performance is expressed in terms of the temperature of the cold plate surface in contact with and this heated by the electronics being cooled. The maximum temperature ($T_{s,max}$) value is used as one of the optimization objectives which influences the maximum temperature of the electronics component. Apart from the maximum temperature, the temperature deviation ($T_{s,dev}$) on the heated surface is used as an optimization objective. The hydraulic performance is mapped in terms of the total pressure drop (ΔP_{tot}) in the cold plate. Therefore, each optimization iteration would require solving for these performance metrics.

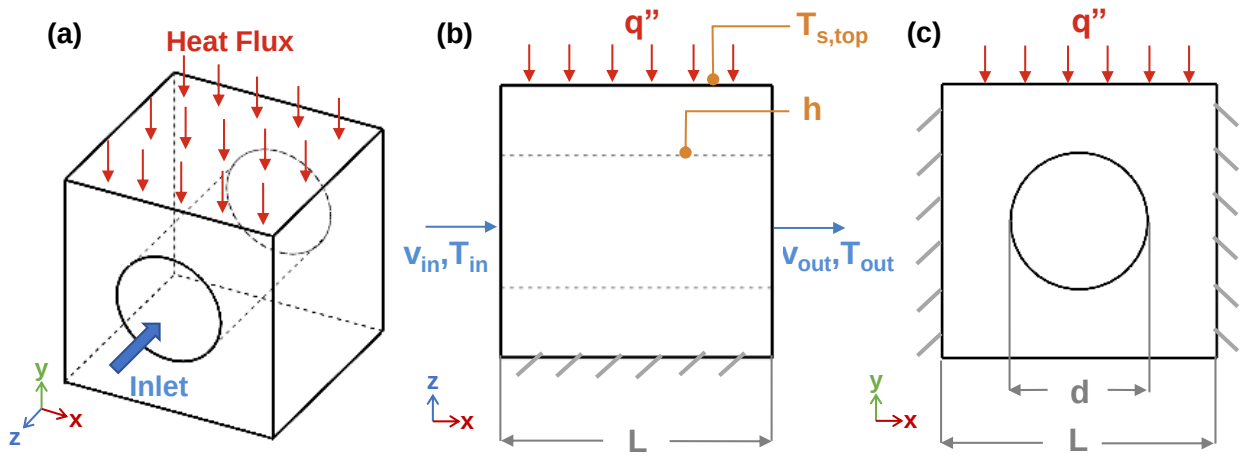

Figure 3.1 (a) Schematic of a straight fluid block element (shown in Fig. 1.1c, top) with a heat flux boundary condition applied to the top surface (red arrows) and coolant entering through one circular face (blue arrow). (b) Side view and (c) Front view of the fluid block showing the boundary conditions and flow and temperature variables.

Fluid flow in each of the flow blocks is modelled as internal channel flow as shown in Figure 3.1. The side view of the flow block shown in Figure 3.1 (b) indicates the constant heat flux

boundary condition ($q" =$ constant) along with the flow and temperature variables including the inlet bulk fluid temperature (T_{in}), average fluid velocity (v_{in}), outlet bulk fluid temperature (T_{out}), average fluid velocity (v_{out}), inner local averaged heat transfer coefficient (h) and the heated surface temperature ($T_{\text{s,top}}$). The fluid block dimension (L) and diameter (d) are presented in the front view of the fluid block shown in Figure 3.1(c). Hatched boundaries indicate adiabatic conditions ($q" = 0$). Flow continuity equation for this block preserves the flow at the inlet and outlet of the block giving:

$$d_{\text{in}}^2 v_{\text{in}} = d_{\text{out}}^2 v_{\text{out}}\,, \tag{1}$$

Where $d_{\text{in}}, v_{\text{in}}$ and $d_{\text{out}}, v_{\text{out}}$ are the channel hydraulic diameter and average flow velocity at the inlet and outlet faces of the flow block, respectively. The momentum conservation for the simple block results in the equation for the element pressure drop given as:

$$\Delta P = \frac{fL}{d}\frac{\rho v^2}{2}\,, \tag{2}$$

ΔP represents the pressure drop within the flow block calculated using f, ρ, L, d, and v which denote friction factor, fluid density, block size/length, average channel hydraulic diameter ($d = (d_{\text{in}} + d_{\text{out}})/2$) and average of the inlet and outlet velocities ($v = (v_{\text{in}} + v_{\text{out}})/2$), respectively.

The continuity equation ensures the conservation of mass entering and leaving each individual block. Momentum conservation provides the pressure drop in terms of the solved velocity values. Here, the Darcy friction factor is used for obtaining the pressure drop in the block in terms of inlet velocity assuming fully hydrodynamically-developed flow. The friction factor is

found according to correlations given in Eqns. (3, 4) for laminar and turbulent flows. Interpolated values are used within the transition regime [49].

$$f = \frac{64}{\mathrm{Re}}; \qquad \mathrm{Re} < 2300 \text{ (Laminar)} \tag{3}$$

$$\frac{1}{\sqrt{f}} = -2\log_{10}\left(\frac{\epsilon}{3.7d} + \frac{2.51}{\mathrm{Re}\sqrt{f}}\right); \quad \mathrm{Re} > 4000 \text{ (Turbulent)} \tag{4}$$

Where Re is the Reynolds number based on average diameter and fluid flow velocity (Re = $\rho v d/\mu$, where μ is the dynamic viscosity of the fluid). The limits on the diameter values prevent drastic changes in flow properties within a single flow block supporting our assumption of a Reynolds number based on average values. Here ϵ is the roughness of the internal surface of the channel. For our simulations, we assumed fairly smooth channels with surface roughness of $\epsilon \approx$ 1.5 μm (drawn Cu tubing).

The heat transfer performance is modeled in terms of fluid temperatures at element boundaries and average temperature of the heated surface for each element. The energy balance for the fluid is given as:

$$\dot{m}C_{\mathrm{p_f}}\left(T_{\mathrm{f,out}} - T_{\mathrm{f,in}}\right) = h_{\mathrm{eff}}A\left(T_{\mathrm{s}} - \frac{T_{\mathrm{f,out}} + T_{\mathrm{f,in}}}{2}\right), \tag{5}$$

Where $C_{\mathrm{p_f}}$ is the fluid specific heat, h_{eff} is the effective heat transfer coefficient between the fluid and heated surface temperature nodes, T_{s} is the temperature at the top surface which is subject to a uniform heat flux (q", Figure 1d) and $T_{\mathrm{f,in}}$, $T_{\mathrm{f,out}}$ are fluid inlet and outlet temperatures respectively. Overall heat transfer coefficient from the fluid to the top surface is obtained using:

$$\frac{1}{h_{\text{eff}}A} = \frac{1}{hA_{\text{c}}} + \frac{1}{k_{\text{s}}S}, \tag{6}$$

Where k_{s} is the thermal conductivity of the solid material and A_{c} and S are the curved internal channel area wetted by fluid and conduction shape factor for heat transfer from the surface to the channel internal wall, respectively. The shape factor correlations are obtained based on parametric simulations conducted prior to simulation of the flow. Here, h is the heat transfer coefficient at the fluid-solid internal channel wall calculated using the following well-validated correlations [50]:

$$\text{Nu} = 4\,, \qquad \text{Laminar} \tag{7}$$

$$\text{Nu} = 0.023\,\text{Re}^{0.8}\text{Pr}^{0.4}, \qquad \text{Turbulent} \tag{8}$$

$$h = \frac{\text{Nu}k_{\text{f}}}{d}. \tag{9}$$

Where Nu is the Nusselt number based on the average hydraulic diameter (d), Pr is the fluid Prandtl Number, and k_{f} is the fluid thermal conductivity. Convective heat transfer in the fluid cannot be modelled with either constant heat flux or constant wall temperature boundary conditions. Hence, an average Nusselt number for flow in a circular channel with constant wall heat flux and constant wall temperature were chosen for the laminar flow regime.

Conduction within the solid domain is considered while solving for the heated surface temperature as:

$$\frac{k_{\text{s}}A_{\text{l}}}{L}\sum_{\text{intenal}}(T_{\text{s}} - T_{\text{nb}}) + h_{\text{amb}}A_{\text{l}}\sum_{\text{corner}}(T_{\text{s}} - T_{\text{amb}}) + \dot{m}C_{\text{f}}\left(T_{\text{f,out}} - T_{\text{f,in}}\right) = q"A_{\text{top}}\,, \tag{10}$$

Where q" is the heat flux, h_{amb} is the heat transfer coefficients to ambient at corner elements, A_{l}, A_{top} are the lateral and top surface areas respectively. The block lateral surface area is assumed to be equal for all faces of the block in contact with neighboring elements or ambient. The bottom surface is assumed to be adiabatic. Here, T_{nb} and T_{amb} denote the neighboring element top surface and ambient temperatures. Effects of heat spreading (lateral block to block heat transfer) within the solid domain is considered within the heat conduction equation. Equations (5) and (10) result in a set of linear equations which are solved to obtain the fluid and heated surface temperature profiles for the entire cold plate. A detailed solution of these equations for an example design on a 2 x 2 design is presented in Appendix A.

The following boundary conditions are used in the optimization processes in the remaining chapters unless otherwise specified. Water is used as a coolant with a mass flow rate of 0.1 kg/s entering the cold plate at 20 ºC. All fluid blocks have the identical dimension $L = 2$ cm. The internal diameters are held constant for the layout optimization at $L = 1$ cm. The cold plate solid material is Aluminum. A uniform heat dissipation of 200 W (q'' = 50 W/cm^2) per grid element is used, except in the cases when the effect of heterogeneous heat dissipation profile is studied.

CHAPTER 4: LAYOUT OPTIMIZATION

The first step in the design optimization is to find an optimal layout representing the coolant flow path in the cold plate. After dividing the domain into a coarse grid, the layout optimization can be viewed as the problem of assigning a flow block for each of the grid elements. As shown in Figure 1.1, the flow blocks for non-parallel designs can be classified as straight and elbows. Within these, depending on the direction of flow inlet and exit, the straight elements can be subclassified into four types and elbows can be subclassified into eight types. Combining these with an empty block with no flow, each of the grid element can be assigned with one of the thirteen unique flow block types. These thirteen flow block types are presented in Figure 4.1.

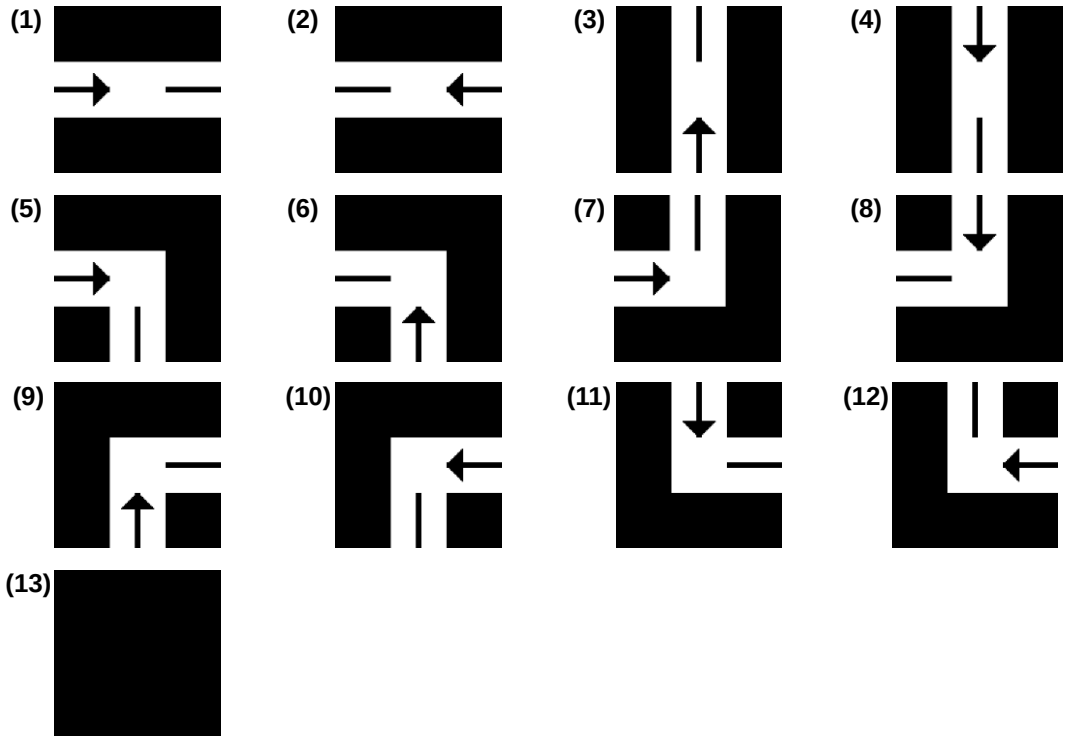

Figure 4.1 Discrete flow block with unique indices used as design variables in layout optimization

The flow block types at all grid locations form the design variables for the layout optimization. As discussed in the previous chapter, the design optimization consists of a multi-objective optimization problem which focuses on both thermal and hydraulic considerations. The optimization problem for minimizing thermal and hydraulic objectives can be formulated as:

$$\min_{\text{layout}} \left(T_{\text{s,max}}, \Delta P_{\text{tot}}, T_{\text{s,dev}}\right), \tag{11}$$

subject to the following conditions:

$$\rho \text{v}_{\text{inlet}} A_{\text{inlet}} = \dot{m}, \tag{12}$$

$$q"(\text{i},\text{j}) = q''_{\text{loss}}. \tag{13}$$

where min represents the multi-variable minimization function over the entire cold plate layout. Here, the maximum top surface temperature among all element blocks $T_{\text{s,max}}$, total pressure drop within entire channel ΔP_{tot} and the standard deviation of the top surface temperatures $T_{\text{s,dev}}$ are minimized with respect to the flow layout using the minimization function. The inlet mass flow rate $\dot{m}$ (Eq. 12) and local heat flux q''_{loss} at individual element locations (i, j, Eq. 13) form the optimization constraints. The multi-objective optimization of $T_{\text{s,max}}$, ΔP and $T_{\text{s,dev}}$ is solved using the unique approach described below.

At each grid element, the flow block can represent any of the thirteen possible types. This implies that even a relatively small grid size of 3 x 4 can have up to 13^{12} possible flow block assignments. As seen from Figure 4.2, not all these assignments lead to a meaningful flow path.

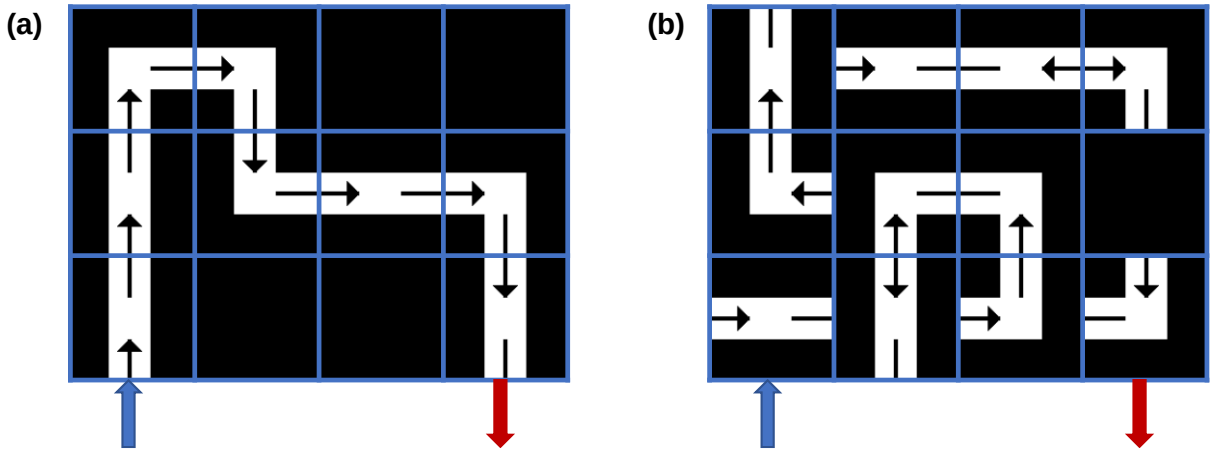

Figure 4.2 3 x 4 grid element assignments with (a) valid and (b) invalid flow layout designs

This implies that for the layout optimization problem, there is a very low probability of finding an optimal flow layout among the large number of possible element assignments making the optimization problem difficult to solve. Identifying the fluid blocks using discrete indices fails to establish similarities between blocks with the same inlet or outlet directions. For instance, flow blocks 1, 5 and 7 all have the flow entering at the west face, but there is no link between the indices for the optimizer to identify this similarity. Establishing such connection between similar elements would help the optimizer take the design from near-valid to valid. The following approach is used to make a connection between elements which have similar flow directions. Each flow block is expressed in terms of four continuous variables, forming two pairs of coordinates. Each pair of coordinates dictates the direction of the flow as depicted in Figure 4.3, depending on the quadrant in which the corresponding point lies in the two-dimensional number line. The two pairs of coordinates represent the direction of the flows on the inlet and outlet of the flow block which in combination corresponds to one of the thirteen unique types. Even though this approach increases the number of design variables for the optimization, it improves the optimization performance by making the objective smoother with respect to the design variables.

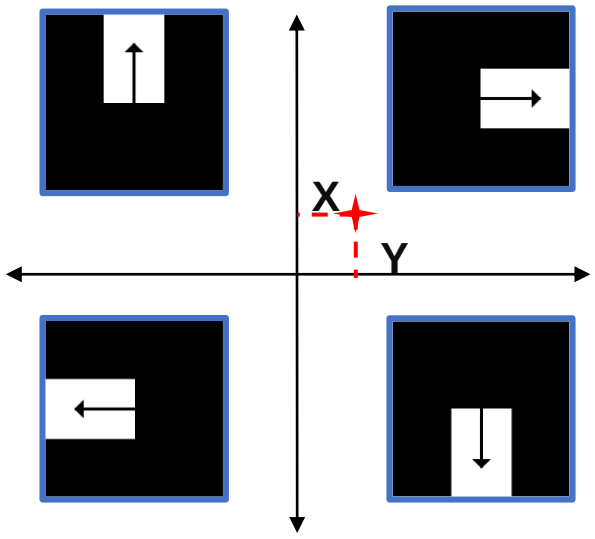

Figure 4.3 Illustration of design variable manipulation to establish connection between similar flow blocks. Identifying outlet flow direction based on a set of coordinates, quadrant I indicates west, quadrant II indicates north, quadrant III indicates east and quadrant IV indicates south.

Another challenge for the optimization process is the disconnect between the performance metrics for valid and invalid designs. Ideally, an invalid design would have infinitely high values of pressure drop and surface temperatures due to the incomplete nature of the flow path, whereas the valid design would have finite values. Thus, making a change at one grid element can take the design from valid to invalid and vice versa. This implies that the objective function would be highly discontinuous with respect to the design variables. To overcome this, partially complete designs need to be identified and assigned with high but finite values of the objectives.

Long continuous chains of the fluid path are identified in terms of a continuity index as shown in Figure 4.4. The continuity index is the measure of the number of elements who are the logical predecessors of the successor elements. For example, Figure 4.4a represents an element with inlet on the same face as that of the outlet face of the predecessor flow block on the left. Figure 4.4b presents a counter example. A discontinuity index keeps track of the logically discontinuous flow blocks.

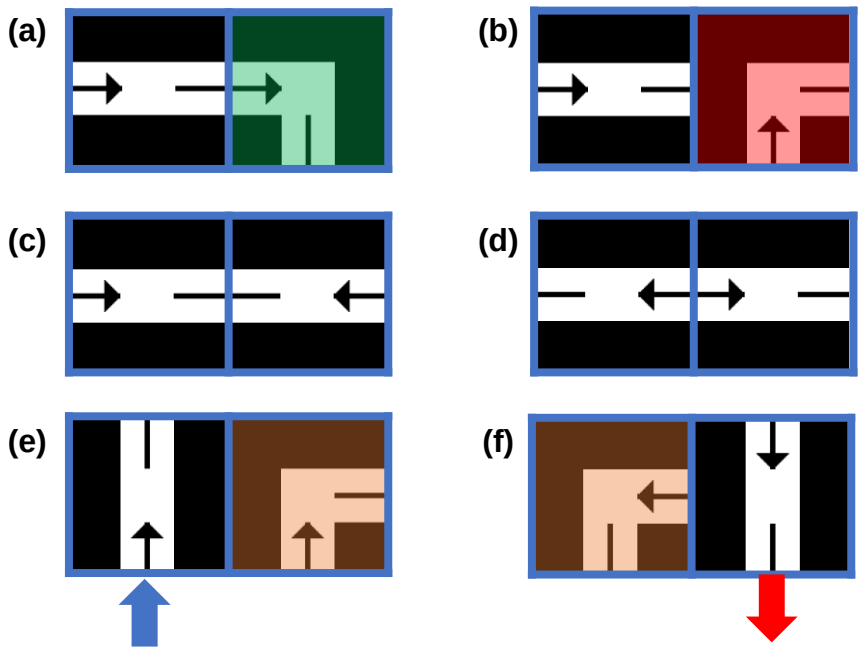

Figure 4.4 Incomplete design penalty metrics (a) continuity index, (b) discontinuity index, (c) converging elements, (d) diverging elements, (e) multiple inlets, (f) multiple outlets

For non-splitting flow paths, converging and diverging elements as shown in figures 4.4c and 4.4d are not permissible. Therefore, the number of instances of converging and diverging elements are recorded as penalty metrics. Similarly, having multiple inlets in the form of flow blocks with inlet facing domain edges as shown in figure 4.4e and multiple outlets as shown in figure 4.4f is penalized. A total design-based penalty term is calculated as a weighted sum of individual penalty metrics discussed above. This total penalty term is used to modify the value of the heat transfer coefficients making an indirect impact on the objective function. This approach of making the objective a relatively smoother function of the design variables makes the optimization problem less challenging for the discrete solvers. The objective gradient is still not a continuous function restricting the use of gradient based optimization solvers. Therefore, Genetic Algorithm (GA) based optimization is used to solve the layout optimization problem.

A Genetic Algorithm (GA) is a type of an evolutionary search algorithm [52]. The GA is effective for discrete optimization problems due to its heuristic search method which does not depend on gradient calculation [53]. The MATLAB-based *ga* function was applied for finding the optimal discrete design variables. At each iteration of the genetic algorithm, the population or the set of design variable vectors consists of the members selected by the following methods. Elite members are the design vectors corresponding to the best values of the objective function. Crossover members are obtained by combination of the parent designs. This combination can have variables corresponding to either of the parent design vectors at all grid locations. The fraction of the crossover members in the design vector population is kept at 20% to ensure the higher degree of randomness in the optimization required. Mutation members are obtained by randomly changing the variables from a parent design vector. A modified mutation function is employed in this work which forces the change of only those variables which correspond to a discontinuous flow block (as shown in Figure 4.4b). This allows for retaining the long continuous flow paths already identified in the optimization process, while trying to correct the discontinuous elements.

Figure 4.5 shows the results of the layout optimization over six attempts for a 3 x 4 grid size. The approach of using multiple runs of the optimizer to improve the probability of finding a global optimal solution is commonly employed in optimization. It is also known as a multi-start approach. A population size of 1000 design variable vectors was chosen. The optimization was terminated if no improvement in the objective value was seen after a 100 iteration. As seen from the results, the optimizer is able to identify long connected fluid paths in most cases but can only find a complete fluid layout connecting prescribed inlet and outlet locations in a few. The difficulty in finding the optimal layout is expected to increase with the number of grid elements, making this method

ineffective solution for the layout optimization problem, thus inspiring the search for alternate methods.

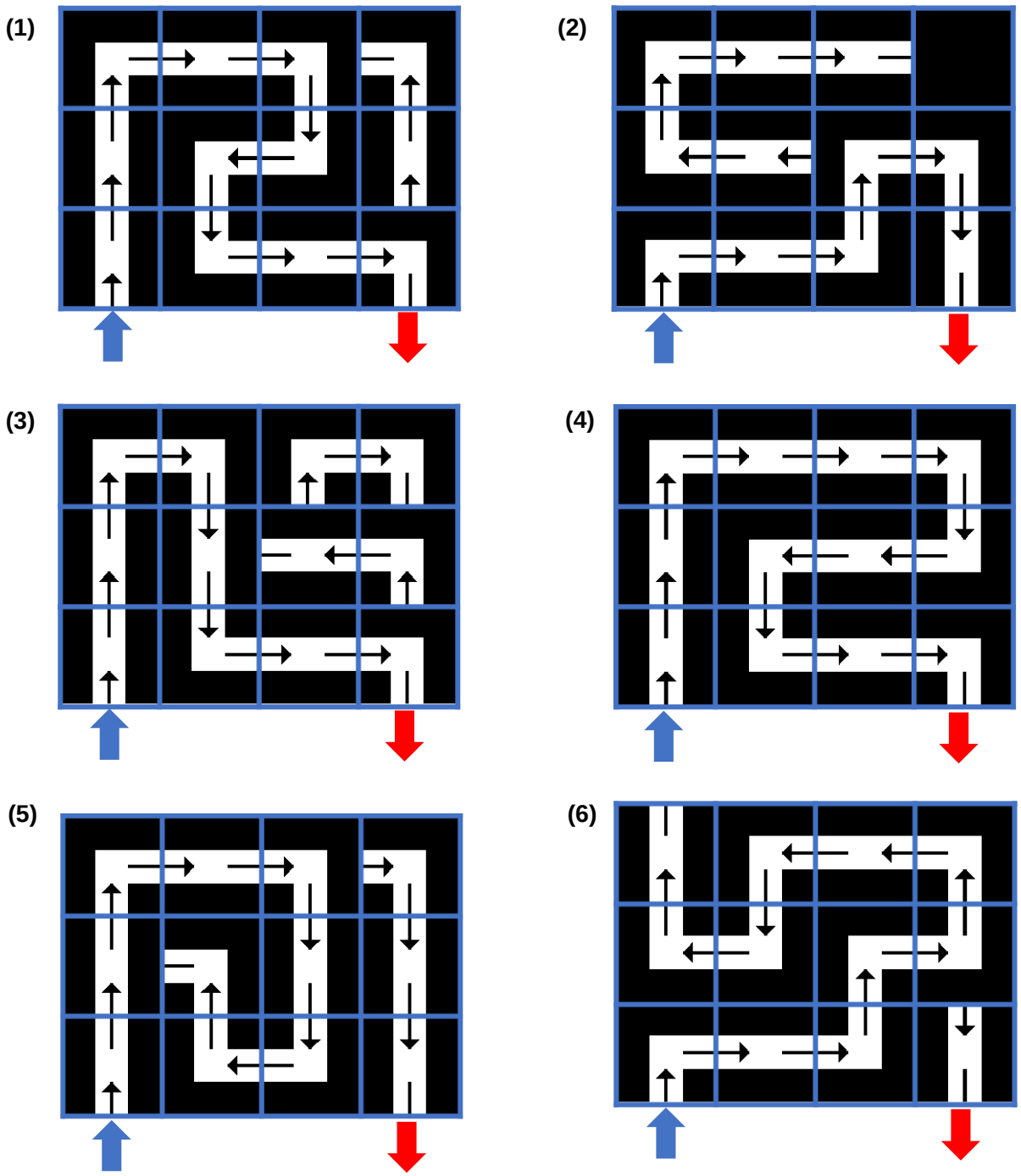

Figure 4.5 Layout optimization results with six runs for a 3 x 4 grid for given inlet (blue arrow) and outlet locations (red arrow). Design 4 represents an example of a complete design.

CHAPTER 5: GEOMETRY OPTIMIZATION

Geometry optimization problem focuses on finding the values of internal flow diameters for a given flow layout and boundary conditions. The optimization formulation is similar to that for the layout optimization presented in equations 11-13 with the design variables changed from the flow layout to the diameters. Contrary to the layout optimization, the objectives are continuous functions of the design variables as seen from Figure 5.1. To generate these trends of objective variation with diameters, the diameters at all grid elements are kept the same. The boundary conditions specified in Chapter 2 are used. To achieve proper scaling of the pressure drop objective, the logarithmic value of the total pressure drop log (ΔP_{tot}) is used. This enables the use of gradient-based optimization solvers which converge to the local optima faster than the gradient free methods like GA. Constrained optimization solver *fmincon* is used to solve the geometry optimization.

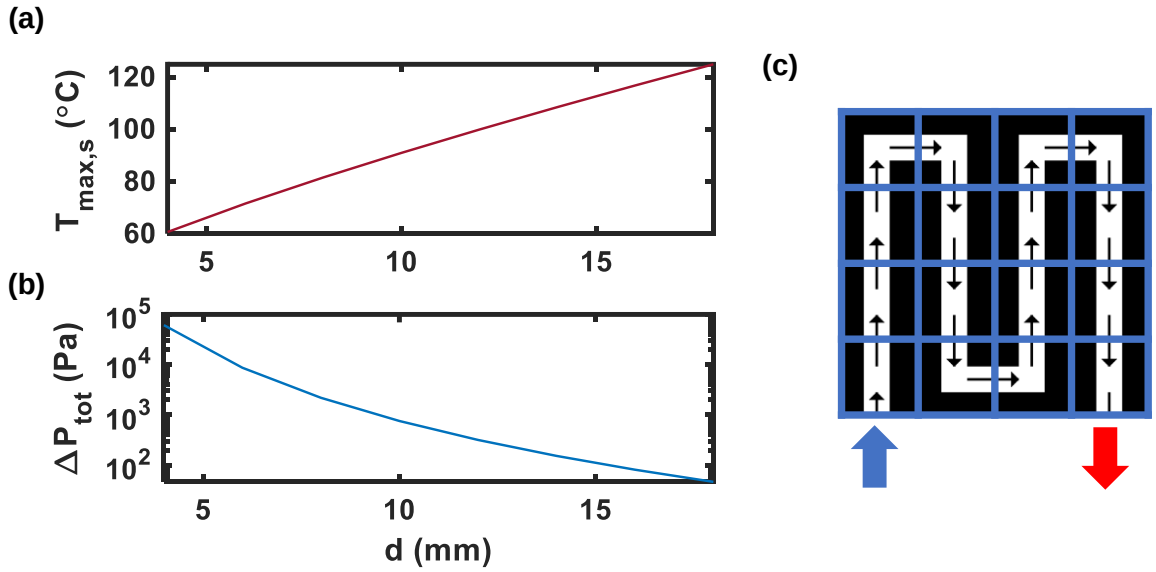

Figure 5.1 Objective functions (a) maximum heated surface temperature ($\boldsymbol{T_{s,max}}$) and (b) total pressure drop ($\boldsymbol{\Delta P_{tot}}$) variation for an (c) exemplary 4x4 flow layout with respect to the internal flow diameters which constitute the design variables for the Geometry Optimization problem

The thermal and hydraulic objective parameters are competing in nature as expected. As the diameters increase, the Darcy friction factor decreases leading to a lower pressure drop. At the same time, the heat transfer coefficient decreases with increasing diameters resulting in higher temperatures. The competing behavior generates a set of pareto-optimal points for the bi-objective optimization. To capture the list of all pareto-optimal points, the pressure drop is constrained by a preset value. This value is varied to get a range of pareto optimal designs forming the pareto front as shown in Figure 5.2. The insets in the plot show optimal designs for different combinations of thermal resistance and pressure drop objectives.

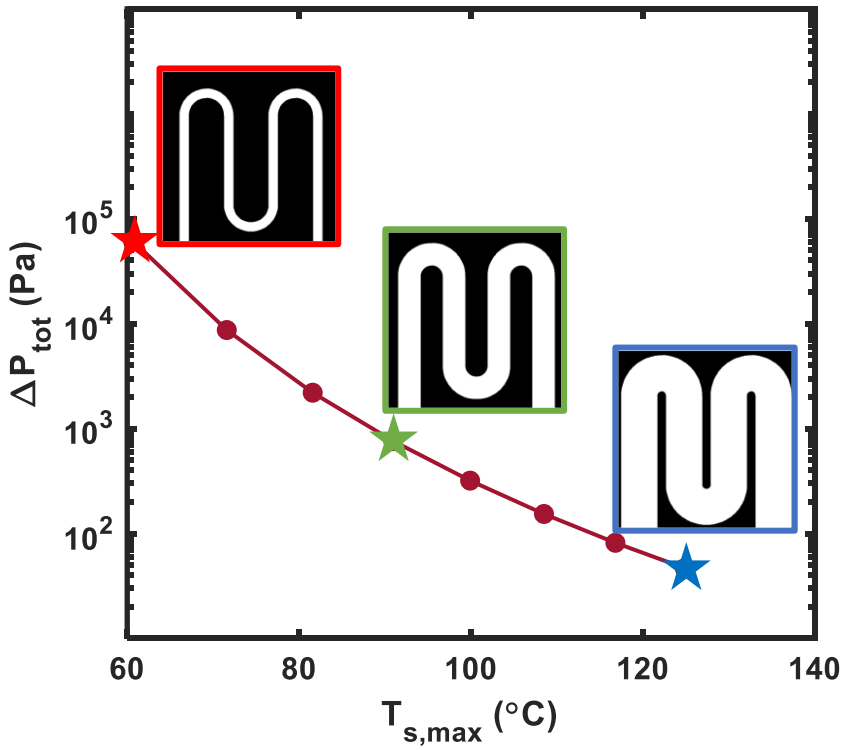

Figure 5.2 Pareto front for bi-objective optimization of maximum surface temperature ($\boldsymbol{T_{s,max}}$) and pressure drop ($\boldsymbol{\Delta P_{tot}}$) using optimization of geometrical parameters (fluid flow block diameters) for the exemplary 4 x 4 flow layout

The optimal geometry is expected to vary with the boundary conditions. As mentioned earlier, electronics cooling applications can lead to a heterogeneous heat dissipation profile on the cold plate surface. This heat dissipation profile is captured by splitting the domain into the coarse grid. Each element of the coarse grid can be assigned with a unique heat dissipation. The effect of heat dissipation profile on optimal diameters with uniform and concentrated profiles is studied. Two heat dissipation cases included uniform and concentrated loss profiles are considered as shown in Figure 5.3.

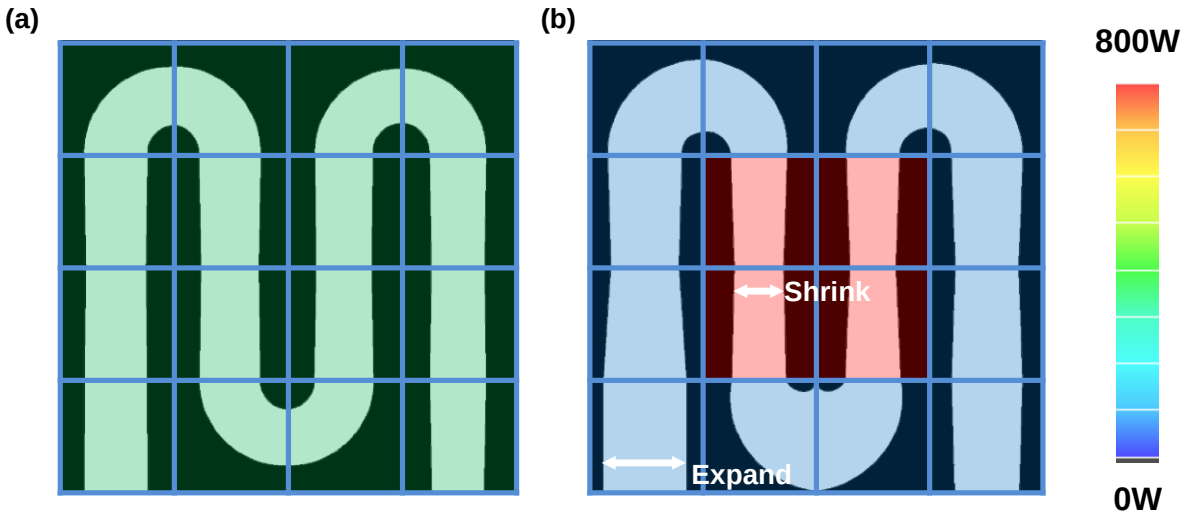

Figure 5.3 Effect of heat dissipation profile on geometry optimization results for the same flow layout with (a) uniform heat dissipation profile with 200W per element and (c) concentrated heat dissipation with 800W on four central elements and zero loss on corner elements.

For the uniform loss profile, all grid elements were assigned a fixed heat dissipation value of 200 W (q'' = 50 W/cm^2). In the concentrated loss case, the four central grid elements were assigned a fixed heat dissipation value of 800 W (q'' = 200 W/cm^2), with all other elements being adiabatic (q'' = 0) ensuring that the total heat dissipation in both cases is identical. In the case of uniform heat dissipation (Figure 5.3a), the optimal diameter values are nearly equal for all element faces, resulting in low pressure drop encountered for the gradual changes in diameters. For the

concentrated heat dissipation profile (Figure 5.3b), the diameter values in the central region where heat dissipations are applied are smaller than the uniform heat dissipation case. The smaller diameters lead to increased local heat transfer coefficients, and also cause higher pressure drop. To counter the elevated pressure drop while maintaining good thermal performance, the optimal design selects larger diameter values in the outer regions of the grid near the edges, with the resulting total pressure drop being similar for both the uniform and concentrated heat dissipation cases. The optimized design improves the maximum surface temperature objective by 4.1% relative to the coolant inlet temperature without significant change in the total pressure drop compared to the design with identical diameters at all grid elements.

The geometry optimization uses the flow layout as an input but is not tied to the layout optimization routine. Geometry optimization can be used independently of the overall cold plate design optimization process if the flow layout is known or inferred from the cold plate design. For the example applications of the geometry optimization on the 4 x 4 designs, the optimizer converges in a timescale of 30 seconds. The computations were performed on an Inlet(R) Core™ i7-10700 CPU @ 2.9GHz computer using serial computing. With the number of grid elements up to 50, the geometry optimization is expected to take up to 60 seconds. The low computation times of the geometry optimization align well with the goal of achieving rapid design optimization of cold plates.

CHAPTER 6: DISCUSSION AND FUTURE WORK

A reduced order framework for optimizing thermal-hydraulic performance metrics of the single-phase liquid cooled heat sinks such as cold plates and microchannel coolers is proposed in this thesis. The overall design optimization is divided into layout optimization and geometry optimization subproblems. Layout optimization problem is inherently discrete and is thus solved using GA with a custom mutation function. The optimization objective formulation and the design variable representation are modified to improve optimization performance. Finding the globally optimal layout is not ensured despite these efforts. A multi-start approach is shown to improve the probability of finding the optimal design, but multiple runs of the optimization solver result in increased computation time making it unsuitable for the rapid design optimization.

The layout optimization can be revisited as a path search problem on the coarse grid dividing the cold plate domain. Heuristic shortest path search algorithms have proven effective for applications in robotics [54] and transportation [55]. Implementing a search method finding the flow layout with the goal of achieving optimal performance could complement the implementation of the discrete optimization algorithm presented in this work. Parallel computing can be employed in future work to reduce the computation time compared to the serial computations used.

Modeling approach used predicts thermal-hydraulic performance on a coarse grid resulting in low computational effort. Although the key assumptions made to develop the simplified modeling approach can result in lower-fidelity estimation of thermal-hydraulic parameters, comparative performance of designs under investigation can be expected to be the same as that obtained using high-fidelity simulation methods. This enables the use of reduced order modeling for design optimization. Despite the non-optimal prediction fidelity, modeling accuracy can be

further improved with the incorporation of correlations developed for flow and temperature parameters using high fidelity CFD simulations.

This work focuses on designs with non-splitting flow layouts (serial channels). Dedicated correlations to differentiate the flow behavior and resulting thermal performance changes in elbows as compared to straight blocks are required. Furthermore, additional development is needed to establish a performance modeling approach that can include flow branching. In addition, the method should be modified to accommodate non-uniform grids to allow local refinement within the cold plate geometry. Layout search and geometry optimization methods also need to be modified to consider parallel flow architectures.

Similar to the simple flow blocks used in this work, correlations can be developed for blocks including performance enhancing aspects such as internal fins and turbulence inducing features. Advanced manufacturing methods including additive manufacturing can make such designs realizable [56]–[61]. In the future, it would be interesting to utilize our tool to conduct additional case studies for practical cooling applications with differing heat dissipation profiles and compare the results with the well-established cooling methods currently used [62]. Furthermore, future work is needed to obtain rigorous design optimization performance benchmarks against state-of-the-art design methods and design optimization software packages (ANSYS, COMSOL) in the context of required computational resources and timescale for identification of an optimal solution.

Two-phase heat sinks for cooling of electronics are a topic of high interest. Flow boiling in channel flow offers potential for achieving higher heat flux removal capabilities when compared to single-phase liquid flow while also providing isothermal cooling [64]–[66]. The coarse meshing approach for performance prediction presented in this work can be translated for heat sinks

undergoing two-phase flow without impacting the computational speeds. This can be achieved with reliable correlations which are available for predicting macro-scale flow and thermal behavior. Reliability of such applications of the tool needs to be validated and improved with the help of high-fidelity simulations [66]–[68] and experimental approaches [69]–[71].

Rapid design optimization creates potential for integration with electro-thermal co-design tools already available [45]–[48]. Traditional approaches mainly rely on detailed thermal analysis based on numerical methods requiring significant time and computational effort. These approaches limit the number of design iterations available for identifying the optimal packaging of electronics. These also require a high level of user expertise in setting up the numerical simulations to ensure accurate results. The methods demonstrated in this work allow for the rapid design of compact electronics packaging systems with high performance cooling solutions. The designs generated using this method can also be used as starting points for high fidelity design optimization using topology optimization.

CHAPTER 7: CONCLUSION

An approach for design of single-phase liquid cooled channel heat sinks can be optimized using limited time and computing resources. Our approach combines modeling on a coarse grid using existing performance correlations for obtaining pressure drop and temperature profiles, flow layout optimization through multiple path searches using randomized populations and gradient-based optimization for cross-section geometries. Modifications to the design representation in terms of optimization variables and objective function for partially complete designs enables achieving an optimal solution for the flow layout using GA. Multiple runs of optimization are still required to improve the probability of finding the global maximum. The geometry optimization problem solves within 60 s for flow diameters for all elements of the coarse grid having up to 50 flow blocks using gradient based optimizers enabled by continuous variation of the objectives with respect to the design variables. The proposed approach can address heterogeneous loss profiles commonly seen in electronics packaging. Optimized geometry for a standard four pass cold plate design has reduced the peak temperature of the heated surface by 4.1% without significant change in the pressure drop. Proposed design framework can potentially incorporate enhancements such as consideration of parallel flow designs, two-phase flows, internal flow features (fins), and non-uniform grids with minor modifications to the performance modeling approach. The reduced-order design optimization presented in this work offers significant benefits in terms of computational and temporal requirements when compared to methods using CFD simulations coupled with numerical optimization. The rapid solution and low computational requirement of this work enable potential design application in electro-thermal co-design for electronics packaging.

REFERENCES

[1] B. Hoefflinger, "ITRS: The International Technology Roadmap for Semiconductors," Springer, Berlin, Heidelberg, 2011, pp. 161–174. doi: 10.1007/978-3-642-23096-7_7.

[2] B. Bilgin *et al.*, "Making the Case for Electrified Transportation," *IEEE Transactions on Transportation Electrification*, vol. 1, no. 1, pp. 4–17, Jun. 2015, doi: 10.1109/TTE.2015.2437338.

[3] S. Sathe and B. Sammakia, "A Review of Recent Developments in Some Practical Aspects of Air-Cooled Electronic Packages," *Journal of Heat Transfer*, vol. 120, no. 4, pp. 830–839, Nov. 1998, doi: 10.1115/1.2825902.

[4] H. Wang, M. Liserre, and F. Blaabjerg, "Toward reliable power electronics: Challenges, design tools, and opportunities," *IEEE Industrial Electronics Magazine*, vol. 7, no. 2, pp. 17–26, 2013, doi: 10.1109/MIE.2013.2252958.

[5] J. Broughton, V. Smet, R. R. Tummala, and Y. K. Joshi, "Review of Thermal Packaging Technologies for Automotive Power Electronics for Traction Purposes," *Journal of Electronic Packaging, Transactions of the ASME*, vol. 140, no. 4, Dec. 2018, doi: 10.1115/1.4040828/366154.

[6] D. B. Tuckerman and R. F. W. Pease, "High-Performance Heat Sinking for VLSI," *IEEE Electron Device Letters*, vol. EDL-2, no. 5, pp. 126–129, 1981, doi: 10.1109/EDL.1981.25367.

[7] A. Weisberg, H. H. Bau, and J. N. Zemel, "Analysis of microchannels for integrated cooling," *International Journal of Heat and Mass Transfer*, vol. 35, no. 10, pp. 2465–2474, Oct. 1992, doi: 10.1016/0017-9310(92)90089-B.

[8] X. F. Peng and G. P. Peterson, "The effect of thermofluid and geometrical parameters on convection of liquids through rectangular microchannels," *International Journal of Heat and Mass Transfer*, vol. 38, no. 4, pp. 755–758, Mar. 1995, doi: 10.1016/0017-9310(95)93010-F.

[9] W. Qu and I. Mudawar, "Experimental and numerical study of pressure drop and heat transfer in a single-phase micro-channel heat sink," *International Journal of Heat and Mass Transfer*, vol. 45, no. 12, pp. 2549–2565, Apr. 2002, doi: 10.1016/S0017-9310(01)00337-4.

[10] R. W. Knight, J. S. Goodling, and D. J. Hall, "Optimal thermal design of forced convection heat sinks-analytical," *Journal of Electronic Packaging, Transactions of the ASME*, vol. 113, no. 3, pp. 313–321, Sep. 1991, doi: 10.1115/1.2905412.

[11] S. J. Kim and D. Kim, “Forced convection in microstructures for electronic equipment cooling,” *Journal of Heat Transfer*, vol. 121, no. 3, pp. 639–645, Aug. 1999, doi: 10.1115/1.2826027.

[12] C. Y. Zhao and T. J. Lu, “Analysis of microchannel heat sinks for electronics cooling,” *International Journal of Heat and Mass Transfer*, vol. 45, no. 24, pp. 4857–4869, Sep. 2002, doi: 10.1016/S0017-9310(02)00180-1.

[13] C. H. Chen, “Forced convection heat transfer in microchannel heat sinks,” *International Journal of Heat and Mass Transfer*, vol. 50, no. 11–12, pp. 2182–2189, Jun. 2007, doi: 10.1016/j.ijheatmasstransfer.2006.11.001.

[14] X. L. Xie, W. Q. Tao, and Y. L. He, “Numerical study of turbulent heat transfer and pressure drop characteristics in a water-cooled minichannel heat sink,” *Journal of Electronic Packaging, Transactions of the ASME*, vol. 129, no. 3, pp. 247–255, Sep. 2007, doi: 10.1115/1.2753887.

[15] X. L. Xie, Z. J. Liu, Y. L. He, and W. Q. Tao, “Numerical study of laminar heat transfer and pressure drop characteristics in a water-cooled minichannel heat sink,” *Applied Thermal Engineering*, vol. 29, no. 1, pp. 64–74, Jan. 2009, doi: 10.1016/j.applthermaleng.2008.02.002.

[16] A. G. Fedorov and R. Viskanta, “Three-dimensional conjugate heat transfer in the microchannel heat sink for electronic packaging,” *International Journal of Heat and Mass Transfer*, vol. 43, no. 3, pp. 399–415, Feb. 2000, doi: 10.1016/S0017-9310(99)00151-9.

[17] L. Chai, G. D. Xia, and H. S. Wang, “Parametric study on thermal and hydraulic characteristics of laminar flow in microchannel heat sink with fan-shaped ribs on sidewalls - Part 1: Heat transfer,” *International Journal of Heat and Mass Transfer*, vol. 97, pp. 1069–1080, Jun. 2016, doi: 10.1016/j.ijheatmasstransfer.2016.02.077.

[18] L. Chai, G. D. Xia, and H. S. Wang, “Parametric study on thermal and hydraulic characteristics of laminar flow in microchannel heat sink with fan-shaped ribs on sidewalls - Part 2: Pressure drop,” *International Journal of Heat and Mass Transfer*, vol. 97, pp. 1081–1090, Jun. 2016, doi: 10.1016/j.ijheatmasstransfer.2016.02.076.

[19] L. Chai, G. D. Xia, and H. S. Wang, “Parametric study on thermal and hydraulic characteristics of laminar flow in microchannel heat sink with fan-shaped ribs on sidewalls - Part 3: Performance evaluation,” *International Journal of Heat and Mass Transfer*, vol. 97, pp. 1091–1101, Jun. 2016, doi: 10.1016/j.ijheatmasstransfer.2016.02.075.

[20] R. W. Knight, J. S. Goodling, D. J. Hall, and R. C. Jaeger, “Heat Sink Optimization with Application to Microchannels,” *IEEE Transactions on Components, Hybrids, and Manufacturing Technology*, vol. 15, no. 5, pp. 832–842, 1992, doi: 10.1109/33.180049.

[21] Y. Murakami and B. B. Mikić, “Parametric optimization of multichanneled heat sinks for VLSI chip cooling,” *IEEE Transactions on Components and Packaging Technologies*, vol. 24, no. 1, pp. 2–9, Mar. 2001, doi: 10.1109/6144.910795.

[22] C. S. Sharma, S. Zimmermann, M. K. Tiwari, B. Michel, and D. Poulikakos, “Optimal thermal operation of liquid-cooled electronic chips,” *International Journal of Heat and Mass Transfer*, vol. 55, no. 7–8, pp. 1957–1969, Mar. 2012, doi: 10.1016/j.ijheatmasstransfer.2011.11.052.

[23] J. Zhang, P. T. Lin, and Y. Jaluria, “Design and optimization of multiple microchannel heat transfer systems,” *Journal of Thermal Science and Engineering Applications*, vol. 6, no. 1, Mar. 2014, doi: 10.1115/1.4024706.

[24] Y. Hadad *et al.*, “Three-objective shape optimization and parametric study of a micro-channel heat sink with discrete non-uniform heat flux boundary conditions,” *Applied Thermal Engineering*, vol. 150, pp. 720–737, Mar. 2019, doi: 10.1016/J.APPLTHERMALENG.2018.12.128.

[25] Y. Sui, C. J. Teo, P. S. Lee, Y. T. Chew, and C. Shu, “Fluid flow and heat transfer in wavy microchannels,” *International Journal of Heat and Mass Transfer*, vol. 53, no. 13–14, pp. 2760–2772, Jun. 2010, doi: 10.1016/j.ijheatmasstransfer.2010.02.022.

[26] Y. Sui, P. S. Lee, and C. J. Teo, “An experimental study of flow friction and heat transfer in wavy microchannels with rectangular cross section,” *International Journal of Thermal Sciences*, vol. 50, no. 12, pp. 2473–2482, Dec. 2011, doi: 10.1016/j.ijthermalsci.2011.06.017.

[27] G. Xie, J. Liu, W. Zhang, and B. Sunden, “Analysis of flow and thermal performance of a water-cooled transversal wavy microchannel heat sink for chip cooling,” *Journal of Electronic Packaging, Transactions of the ASME*, vol. 134, no. 4, Dec. 2012, doi: 10.1115/1.4023035.

[28] X. Hao, B. Peng, G. Xie, and Y. Chen, “Thermal analysis and experimental validation of laminar heat transfer and pressure drop in serpentine channel heat sinks for electronic cooling,” *Journal of Electronic Packaging, Transactions of the ASME*, vol. 136, no. 3, Sep. 2014, doi: 10.1115/1.4027508.

[29] Z. Dai, D. F. Fletcher, and B. S. Haynes, “Impact of tortuous geometry on laminar flow heat transfer in microchannels,” *International Journal of Heat and Mass Transfer*, vol. 83, pp. 382–398, Apr. 2015, doi: 10.1016/j.ijheatmasstransfer.2014.12.019.

[30] A. F. Al-Neama, N. Kapur, J. Summers, and H. M. Thompson, “An experimental and numerical investigation of the use of liquid flow in serpentine microchannels for microelectronics cooling,” *Applied Thermal Engineering*, vol. 116, pp. 709–723, Apr. 2017, doi: 10.1016/j.applthermaleng.2017.02.001.

[31] A. Iga, S. Nishiwaki, K. Izui, and M. Yoshimura, “Topology optimization for thermal conductors considering design-dependent effects, including heat conduction and convection,” *International Journal of Heat and Mass Transfer*, vol. 52, no. 11–12, pp. 2721–2732, May 2009, doi: 10.1016/j.ijheatmasstransfer.2008.12.013.

[32] G. H. Yoon, “Topological design of heat dissipating structure with forced convective heat transfer,” *Journal of Mechanical Science and Technology*, vol. 24, no. 6, pp. 1225–1233, 2010, doi: 10.1007/s12206-010-0328-1.

[33] J. Alexandersen, N. Aage, C. S. Andreasen, and O. Sigmund, “Topology optimisation for natural convection problems,” *International Journal for Numerical Methods in Fluids*, vol. 76, no. 10, pp. 699–721, Dec. 2014, doi: 10.1002/fld.3954.

[34] E. M. Dede, “Optimization and design of a multipass branching microchannel heat sink for electronics cooling,” *Journal of Electronic Packaging, Transactions of the ASME*, vol. 134, no. 4, Dec. 2012, doi: 10.1115/1.4007159.

[35] A. A. Koga, E. C. C. Lopes, H. F. Villa Nova, C. R. D. Lima, and E. C. N. Silva, “Development of heat sink device by using topology optimization,” *International Journal of Heat and Mass Transfer*, vol. 64, pp. 759–772, Sep. 2013, doi: 10.1016/j.ijheatmasstransfer.2013.05.007.

[36] S. Yan, F. Wang, J. Hong, and O. Sigmund, “Topology optimization of microchannel heat sinks using a two-layer model,” *International Journal of Heat and Mass Transfer*, vol. 143, p. 118462, Nov. 2019, doi: 10.1016/j.ijheatmasstransfer.2019.118462.

[37] X. Dong and X. Liu, “Multi-objective optimal design of microchannel cooling heat sink using topology optimization method,” *Numerical Heat Transfer; Part A: Applications*, vol. 77, no. 1, pp. 90–104, Jan. 2020, doi: 10.1080/10407782.2019.1682872.

[38] H. Li, X. Ding, F. Meng, D. Jing, and M. Xiong, “Optimal design and thermal modelling for liquid-cooled heat sink based on multi-objective topology optimization: An experimental and numerical study,” *International Journal of Heat and Mass Transfer*, vol. 144, p. 118638, Dec. 2019, doi: 10.1016/j.ijheatmasstransfer.2019.118638.

[39] J. S. Lee, S. Y. Yoon, B. Kim, H. Lee, M. Y. Ha, and J. K. Min, “A topology optimization based design of a liquid-cooled heat sink with cylindrical pin fins having varying pitch,” *International Journal of Heat and Mass Transfer*, vol. 172, p. 121172, Jun. 2021, doi: 10.1016/j.ijheatmasstransfer.2021.121172.

[40] T. Laurila *et al.*, “Evolution of microstructure and failure mechanism of lead-free solder interconnections in power cycling and thermal shock tests,” *Microelectronics Reliability*, vol. 47, no. 7, pp. 1135–1144, Jul. 2007, doi: 10.1016/j.microrel.2006.07.095.

[41] K. N. Subramanian, “Reliability of Lead-Free Electronic Solder Interconnects: Roles of Material and Service Parameters,” in *Lead-free Solders: Materials Reliability for Electronics,* Wiley Blackwell, 2012, pp. 2–9. doi: 10.1002/9781119966203.ch1.

[42] Y. J. Lee, P. S. Lee, and S. K. Chou, “Hotspot mitigating with obliquely finned microchannel heat sink-an experimental study,” *IEEE Transactions on Components, Packaging and Manufacturing Technology*, vol. 3, no. 8, pp. 1332–1341, 2013, doi: 10.1109/TCPMT.2013.2244164.

[43] C. S. Sharma *et al.*, “Energy efficient hotspot-targeted embedded liquid cooling of electronics,” *Applied Energy*, vol. 138, pp. 414–422, Jan. 2015, doi: 10.1016/j.apenergy.2014.10.068.

[44] C. S. Sharma, G. Schlottig, T. Brunschwiler, M. K. Tiwari, B. Michel, and D. Poulikakos, “A novel method of energy efficient hotspot-targeted embedded liquid cooling for electronics: An experimental study,” *International Journal of Heat and Mass Transfer*, vol. 88, pp. 684–694, Sep. 2015, doi: 10.1016/j.ijheatmasstransfer.2015.04.047.

[45] Y. Park *et al.*, “Electro-thermal co-design of a cooling system-integrated high-frequency transformer,” in *2020 IEEE Transportation Electrification Conference and Expo, ITEC 2020*, Jun. 2020, pp. 26–31. doi: 10.1109/ITEC48692.2020.9161660.

[46] M. Deckard, P. Shamberger, M. Fish, M. Berman, J. Wang, and L. Boteler, “Convergence and validation in parapower: A design tool for phase change materials in electronics packaging,” in *InterSociety Conference on Thermal and Thermomechanical Phenomena in Electronic Systems, ITHERM*, May 2019, vol. 2019-May, pp. 878–885. doi: 10.1109/ITHERM.2019.8757334.

[47] A. Razi, Q. Le, T. M. Evans, S. Mukherjee, H. A. Mantooth, and Y. Peng, “PowerSynth Design Automation Flow for Hierarchical and Heterogeneous 2.5-D Multichip Power Modules,” *IEEE TRANSACTIONS ON POWER ELECTRONICS*, vol. 36, no. 8, 2021, doi: 10.1109/TPEL.2021.3049776.

[48] G. Mademlis, R. Orbay, Y. Liu, N. Sharma, R. Arvidsson, and T. Thiringer, “Multidisciplinary cooling design tool for electric vehicle SiC inverters utilizing transient 3D-CFD computations,” *eTransportation*, vol. 7, p. 100092, Feb. 2021, doi: 10.1016/j.etran.2020.100092.

[49] Frank M. White, *Fluid Mechanics*, 4th Edition. McGraw-Hill International, 1999.

[50] Bergman T.L., Levine A.S., Incropera F.P., and Dewitt D.P., *Fundamentals of Heat and Mass Transfer*, 7th Edition. John Wiley & Sons, 2011.

[51] “Wakefield Thermal Cold Heat Sink 180-20 152.4mm x 139.7mm - 180-20-6C.” https://wakefieldthermal.com/wakefield-thermal-cold-plate-heatsink-0-038c-w-180-20-6c/ (accessed Apr. 11, 2022).

[52] D. E. Goldberg, “Genetic and evolutionary algorithms come of age,” *Commun ACM*, vol. 37, no. 3, pp. 113–120, Mar. 1994, Accessed: Jun. 13, 2021. [Online]. Available: https://go.gale.com/ps/i.do?p=AONE&sw=w&issn=00010782&v=2.1&it=r&id=GALE%7CA15061357&sid=googleScholar&linkaccess=fulltext

[53] J. S. Arora, M. W. Huang, and C. C. Hsieh, “Review Papers Methods for optimization variables: a review of nonlinear problems with discrete,” Springer-Verlag, 1994.

[54] K. Karur, N. Sharma, C. Dharmatti, and J. E. Siegel, “A Survey of Path Planning Algorithms for Mobile Robots,” *Vehicles 2021, Vol. 3, Pages 448-468*, vol. 3, no. 3, pp. 448–468, Aug. 2021, doi: 10.3390/VEHICLES3030027.

[55] M. R. Hribar, V. E. Taylor, and D. E. Boyce, “Implementing parallel shortest path for parallel transportation applications,” *Parallel Computing*, vol. 27, no. 12, pp. 1537–1568, Nov. 2001, doi: 10.1016/S0167-8191(01)00105-3.

[56] B. Kwon, T. Foulkes, T. Yang, N. Miljkovic, and W. P. King, “Air Jet Impingement Cooling of Electronic Devices Using Additively Manufactured Nozzles,” *IEEE Transactions on Components, Packaging and Manufacturing Technology*, vol. 10, no. 2, pp. 220–229, Feb. 2020, doi: 10.1109/TCPMT.2019.2936852.

[57] H. Moon, N. Miljkovic, and W. P. King, “High power density thermal energy storage using additively manufactured heat exchangers and phase change material,” *International Journal of Heat and Mass Transfer*, vol. 153, p. 119591, Jun. 2020, doi: 10.1016/j.ijheatmasstransfer.2020.119591.

[58] A. C. Iradukunda, A. Vargas, D. Huitink, and D. Lohan, “Transient thermal performance using phase change material integrated topology optimized heat sinks,” *Applied Thermal Engineering*, vol. 179, p. 115723, Oct. 2020, doi: 10.1016/j.applthermaleng.2020.115723.

[59] A. N. Pilagatti, G. Piscopo, E. Atzeni, L. Iuliano, and A. Salmi, “Design of additive manufactured passive heat sinks for electronics,” *Journal of Manufacturing Processes*, vol. 64, pp. 878–888, Apr. 2021, doi: 10.1016/j.jmapro.2021.01.035.

[60] H. Moon, K. Boyina, N. Miljkovic, and W. P. King, “Heat Transfer Enhancement of Single-Phase Internal Flows using Shape Optimization and Additively Manufactured Flow Structures,” *International Journal of Heat and Mass Transfer*, vol. 177, p. 121510, Oct. 2021, doi: 10.1016/j.ijheatmasstransfer.2021.121510.

[61] J. Y. Ho, P. Liu, K. C. Leong, T. N. Wong, and N. Miljkovic, “A theoretical analysis and parametric study of filmwise condensation on three-dimensional pin fins,” *International Journal of Heat and Mass Transfer*, vol. 171, p. 121092, Jun. 2021, doi: 10.1016/j.ijheatmasstransfer.2021.121092.

[62] D. Agonafer, M. S. Spector, and N. Miljkovic, “Materials and Interface Challenges in High Vapor Quality Two-Phase Flow Boiling Research,” *IEEE Transactions on*

Components, Packaging and Manufacturing Technology, pp. 1–1, 2021, doi: 10.1109/TCPMT.2021.3085255.

[63] I. Mudawar, "Two-Phase Microchannel Heat Sinks: Theory, Applications, and Limitations," *Journal of Electronic Packaging*, vol. 133, no. 4, Dec. 2011, doi: 10.1115/1.4005300.

[64] S. G. Kandlikar, "History, Advances, and Challenges in Liquid Flow and Flow Boiling Heat Transfer in Microchannels: A Critical Review," *Journal of Heat Transfer*, vol. 134, no. 3, Mar. 2012, doi: 10.1115/1.4005126.

[65] N. V. Upot, A. Mahvi, K. F. Rabbi, J. Li, A. M. Jacobi, and N. Miljkovic, "Scalable and Resilient Etched Metallic Micro- and Nanostructured Surfaces for Enhanced Flow Boiling," *ACS Applied Nano Materials*, vol. 2021, p. 6658, 2021, doi: 10.1021/ACSANM.1C00524.

[66] D. Lorenzini and Y. K. Joshi, "CFD Analysis of Flow Boiling in a Silicon Microchannel With Non-Uniform Heat Flux," *ASME 2015 13th International Conference on Nanochannels, Microchannels, and Minichannels, ICNMM 2015, collocated with the ASME 2015 International Technical Conference and Exhibition on Packaging and Integration of Electronic and Photonic Microsystems*, Nov. 2015, doi: 10.1115/ICNMM2015-48098.

[67] D. Lorenzini and Y. Joshi, "Numerical modeling and experimental validation of two-phase microfluidic cooling in silicon devices for vertical integration of microelectronics," *International Journal of Heat and Mass Transfer*, vol. 138, pp. 194–207, Aug. 2019, doi: 10.1016/J.IJHEATMASSTRANSFER.2019.04.036.

[68] Z. Pan, J. A. Weibel, and S. v Garimella, "A Cost-Effective Modeling Approach for Simulating Phase Change and Flow Boiling in Microchannels," 2015, Accessed: Aug. 02, 2021. [Online]. Available: https://proceedings.asmedigitalcollection.asme.org

[69] D. Bogojevic *et al.*, "EXPERIMENTAL INVESTIGATION OF NON-UNIFORM HEATING ON FLOW BOILING INSTABILITIES IN A MICROCHANNELS BASED HEAT SINK".

[70] J. Lee and I. Mudawar, "Low-temperature two-phase micro-channel cooling for high-heat-flux thermal management of defense electronics," *2008 11th IEEE Intersociety Conference on Thermal and Thermomechanical Phenomena in Electronic Systems, I-THERM*, pp. 132–144, 2008, doi: 10.1109/ITHERM.2008.4544263.

[71] C. A. Konishi, W. Qu, B. Jasperson, F. E. Pfefferkorn, and K. T. Turner, "Experimental Study of Adiabatic Water Liquid-Vapor Two-Phase Pressure Drop Across an Array of Staggered Micro-Pin-Fins," *ASME International Mechanical Engineering Congress and Exposition, Proceedings*, vol. 10, no. PART C, pp. 1597–1605, Aug. 2009, doi: 10.1115/IMECE2008-69051.

APPENDIX A: REDUCED MODELING EXAMPLE

The reduced order modeling approach for estimating the thermal and hydraulic performance metrics for internal channel flow cold plates is presented in Chapter 3. Cold plate design domain is divided into a coarse grid and fluid blocks are assigned for each grid element as shown in Figure 2.1. Thermal performance is mapped in terms of the cold plate surface temperature. Coolant pressure drop across the cold plate inlet and outlet ports is used as a metric for hydraulic performance. An example of the resulting equations and solution method solving for these parameters for a 2 x 2 design shown in Figure A.1.

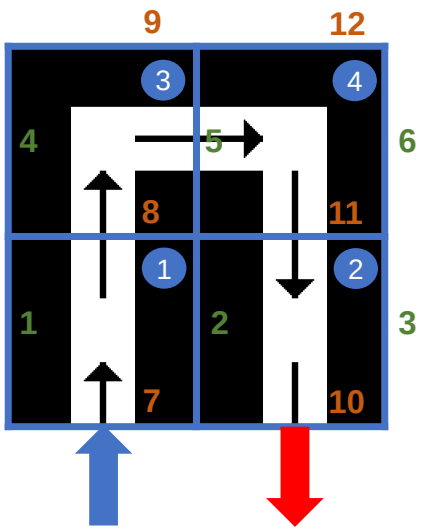

Figure A.1 2 x 2 design example used for demonstrating modeling approach, blue and red arrow represent coolant inlet and outlet locations, vertical and horizontal face indices are shown using green and blue numbers, grid element indices shown in blue circles

The flow variables including the fluid velocity, pressure and fluid temperature at all faces are used. Heated surface temperatures in the solid regions are specified at all grid locations. The following set of equations are used to calculate the velocity values at all faces.

$$d_7^2 v_7 = f(\dot{Q}_{\text{in}}) \tag{A1}$$

$$d_8^2 v_8 = d_7^2 v_7 \tag{A2}$$

$$d_5^2 v_5 = d_8^2 v_8$$

$$d_{11}^2 v_{11} = d_5^2 v_5$$

$$d_{10}^2 v_{10} = d_{11}^2 v_{11}$$

$$v_1 = 0 \tag{A3}$$

$$v_2 = 0$$

$$v_3 = 0$$

$$v_4 = 0$$

$$v_6 = 0$$

$$v_9 = 0$$

$$v_{12} = 0$$

At face 7, the inlet velocity is calculated in terms of the inlet flow rate $\dot{Q}_{\text{in}}$ as shown in equation A1. At subsequent faces with flow, the continuity (equation 1) is used to find the velocities as shown in equation set A2. Velocities at the faces representing internal and domain edge walls are zero as shown in equation set A3. These linear equations can be solved to get the velocity values. The following set of equations solve for the pressures at element faces.

$$p_7 - p_8 = K_{\text{f}} \frac{d\rho_{\text{f}}}{2L} (v_7 + v_8)^2 \tag{A4}$$

$$p_8 - p_5 = K_{\text{f}} \frac{d\rho_{\text{f}}}{2L} (v_8 + v_5)^2$$

$$p_5 - p_{11} = K_{\text{f}} \frac{d\rho_{\text{f}}}{2L} (v_5 + v_{11})^2$$

$$p_{11} - p_{10} = K_{\mathrm{f}} \frac{d\rho_{\mathrm{f}}}{2L} (v_{11} + v_{10})^2$$

$$p_{10} = p_{\mathrm{out}} = 0 \tag{A5}$$

$$p_1 = 0 \tag{A6}$$

$$p_2 = 0$$

$$p_3 = 0$$

$$p_4 = 0$$

$$p_6 = 0$$

$$p_9 = 0$$

$$p_{12} = 0$$

The pressure differences between the active faces (where the fluid is present) are obtained in terms of the previously computed velocity values based on the simplified momentum conservation (equation 2) as shown in equation set A4. The required friction factor values are obtained using equation 3 and 4. Outlet face pressure in equation A5 assumed to be zero to represent the free surface boundary condition. For domain edge and internal walls having no flow, the pressures are set to zero as shown in equation set A6. These equations are solved to estimate the pressures at all element faces. Pressure value at the inlet face is used as the total pressure drop value in the optimization objectives.

The temperatures of the fluid at all faces and the heated surface at all elements are linked as shown in equations 5 and 10 and need to be solved simultaneously. Resulting coupled energy equations for the 2 x 2 design are presented below.

$$C_{\mathrm{f7,8}}(T_{\mathrm{f8}} - T_{\mathrm{f7}}) = C_{\mathrm{etof7,8}}(T_{\mathrm{s,1}} - \frac{T_{\mathrm{f7}} + T_{\mathrm{f8}}}{2}) \tag{A7}$$

$$C_{\mathrm{f8,5}}(T_{\mathrm{f5}} - T_{\mathrm{f8}}) = C_{\mathrm{etof8,5}}(T_{\mathrm{s,3}} - \frac{T_{\mathrm{f8}} + T_{\mathrm{f5}}}{2})$$

$$C_{\mathrm{f5,11}}(T_{\mathrm{f11}} - T_{\mathrm{f5}}) = C_{\mathrm{etof5,11}}(T_{\mathrm{s,4}} - \frac{T_{\mathrm{f5}} + T_{\mathrm{f11}}}{2})$$

$$C_{\mathrm{f11,10}}(T_{\mathrm{f10}} - T_{\mathrm{f11}}) = C_{\mathrm{etof11,10}}(T_{\mathrm{s,2}} - \frac{T_{\mathrm{f11}} + T_{\mathrm{f10}}}{2})$$

$$C_{\mathrm{etonb}}(T_{\mathrm{s,1}} - T_{\mathrm{s,2}}) + C_{\mathrm{etonb}}(T_{\mathrm{s,1}} - T_{\mathrm{s,3}}) + 2C_{\mathrm{etoamb}}(T_{\mathrm{s,1}} - T_{\mathrm{amb}}) + C_{\mathrm{f7,8}}(T_{\mathrm{f8}} - T_{\mathrm{f7}}) = Q_1 \quad \text{(A8)}$$

$$C_{\mathrm{etonb}}(T_{\mathrm{s,3}} - T_{\mathrm{s,1}}) + C_{\mathrm{etonb}}(T_{\mathrm{s,3}} - T_{s,4}) + 2C_{\mathrm{etoamb}}(T_{\mathrm{s,3}} - T_{\mathrm{amb}}) + C_{\mathrm{f8,5}}(T_{\mathrm{f5}} - T_{\mathrm{f8}}) = Q_3$$

$$C_{\mathrm{etonb}}(T_{\mathrm{s,4}} - T_{\mathrm{s,2}}) + C_{\mathrm{etonb}}(T_{\mathrm{s,4}} - T_{\mathrm{s,3}}) + 2C_{\mathrm{etoamb}}(T_{\mathrm{s,4}} - T_{\mathrm{amb}}) + C_{\mathrm{f5,11}}(T_{\mathrm{f11}} - T_{\mathrm{f5}}) = Q_4$$

$$C_{\mathrm{etonb}}(T_{\mathrm{s,2}} - T_{\mathrm{s,3}}) + C_{\mathrm{etonb}}(T_{\mathrm{s,2}} - T_4) + 2C_{\mathrm{etoamb}}(T_{\mathrm{s,2}} - T_{\mathrm{amb}}) + C_{\mathrm{f11,10}}(T_{\mathrm{f10}} - T_{\mathrm{f11}}) = Q_2$$

$$T_{\mathrm{f7}} = T_{\mathrm{f},in} \quad \text{(A9)}$$

$$T_{\mathrm{f1}} = 0 \quad \text{(A10)}$$

$$T_{\mathrm{f2}} = 0$$

$$T_{\mathrm{f3}} = 0$$

$$T_{\mathrm{f4}} = 0$$

$$T_{\mathrm{f6}} = 0$$

$$T_{\mathrm{f9}} = 0$$

$$T_{\mathrm{f12}} = 0$$

In these equations, T_s is the heated surface temperature and T_f is the fluid temperature. Q denotes the heat dissipation applied. Equation set A7 and A8 represent the fluid and solid domain energy conservations respectively. Constant fluid inlet temperature condition is used as specified in equation A9. Temperatures at domain edge and internal wall faces don't contribute to the conservation equations and are assigned a zero value. By specifying unique value for Q at each grid element, we can express the heterogeneous dissipation profiles. Description of the heat transfer capacity values used in solving for temperatures are presented below.

$$C_f = \dot{m} C_p = \rho C_p \pi \frac{d_{in}^2 v_{in} + d_{out}^2 v_{out}}{8} \tag{A11}$$

$$C_{etof} = \frac{1}{R_h + R_c} = \frac{1}{\frac{1}{h\pi \frac{d_{in} + d_{out}}{2} L} + \frac{1}{Sk_s}} \tag{A12}$$

$$C_{etonb} = k_s L \tag{A13}$$

$$C_{etoamb} = h_{amb} L^2 \tag{A14}$$

where C_f is the heat capacity of the fluid, C_{etof} is the heat transfer capacity from fluid to the top surface, C_{etonb} is the heat transfer capacity from solid to its neighboring solid elements and C_{etoamb} is the heat transfer capacity from solid to ambient. The heat transfer coefficient in equation A12 is obtained using the correlations given in equations 7 – 9. h_{amb} is the heat transfer coefficient from solid to ambient which is assigned a low value of $5\ W/m^2K$.

Linear equations A7 - 10 are solved to get the temperature profile on the heated surface. Fluid outlet temperature can also be obtained with this method. Along with the pressure drop, the maximum and deviations of the surface temperature values form the performance metrics for the design and optimization.